Supporting Information

Thermoresponsive Gel Embedding Adipose Stem Cell-Derived Extracellular Vesicles Promotes Esophageal Fistula Healing in a Thermo-Actuated Delivery Strategy

Amanda K. A. Silva[1‡], Silvana Perretta[2‡], Guillaume Perrod[3], Laetitia Pidial[3], Véronique Lindner[4], Florent Carn[1], Shony Lemieux[1], Damien Alloyeau[5], Imane Boucenna[1], Philippe Menasché[6], Bernard Dallemagne[2], Florence Gazeau[1], Claire Wilhelm[1], Christophe Cellier[8], Olivier Clément[3,7], Gabriel Rahmi[3,8*]*

1. Laboratoire Matières et Systèmes Complexes (MSC), UMR 7057 CNRS, Université Sorbonne Paris Cité (USPC), Université Paris-Diderot, 10 rue Alice Domon et Léonie Duquet, 75205 Paris cedex 13, France.

2. Department of Digestive and Endocrine Surgery, Hôpital Civil de Strasbourg, and Institut de Recherche contre les Cancers de l'Appareil Digestif (IRCAD), Strasbourg, France. IHU, Minimally Invasive Hybrid Surgical Institute, Strasbourg, France.

3. Laboratoire Imagerie de l'Angiogénèse, Plateforme d'Imagerie du Petit Animal, PARCC, INSERM U970, Université Sorbonne Paris Cité (USPC), Université Paris Descartes, 56 rue Leblanc, 75015, 75015, Paris, France.

4. Department of Pathology, Hôpital Hautepierre, 1, Avenue Molière, 67098 Strasbourg, France.

5. Laboratoire Matériaux et Phénomènes Quantiques (MPQ), UMR 7162 CNRS/Université Paris - Diderot, 10 rue Alice Domon et Léonie Duquet, 75205 Paris cedex 13, France.

6. Department of Cardiovascular Surgery, Hôpital Européen Georges Pompidou; Paris Cardiovascular Research Center, INSERM U970, Université Paris Descartes, Paris, 75015 France.

7. Department of Radiology, Hôpital Européen Georges Pompidou, Assistance Publique Hôpitaux de Paris, Université Paris Descartes, 20 rue Leblanc, 75015, Paris, France.

8. Gastroenterology and Endoscopy Department, Hôpital Européen Georges Pompidou, Assistance Publique Hôpitaux de Paris, Université Paris Descartes, 20 rue Leblanc, 75015, Paris, France.

‡These authors contributed equally

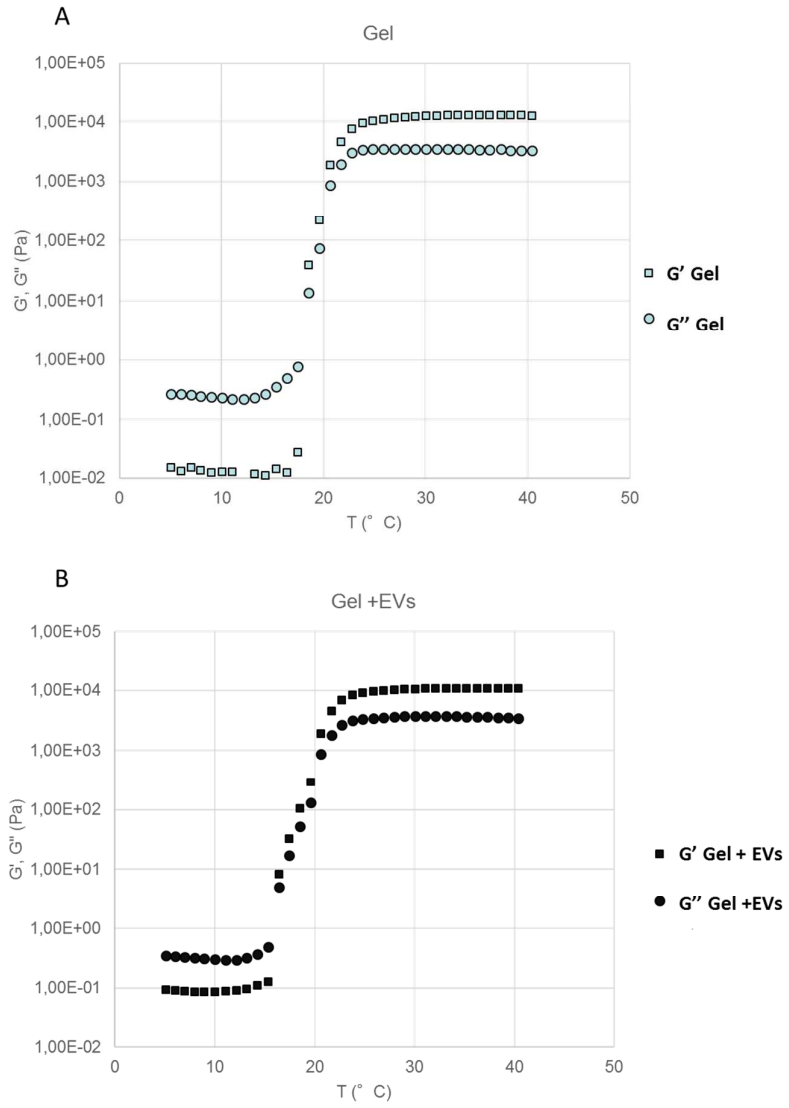

Supplementary Figure 1: Evolution of dynamic storage modulus (G') and loss modulus (G'') at a heating rate of 5°C/min from 5 °C to 40 °C for replicate samples of Pluronic F127 gel at 20% and Pluronic F127 gel at 20% containing $1.3x10^{11}$ EVs/ml.

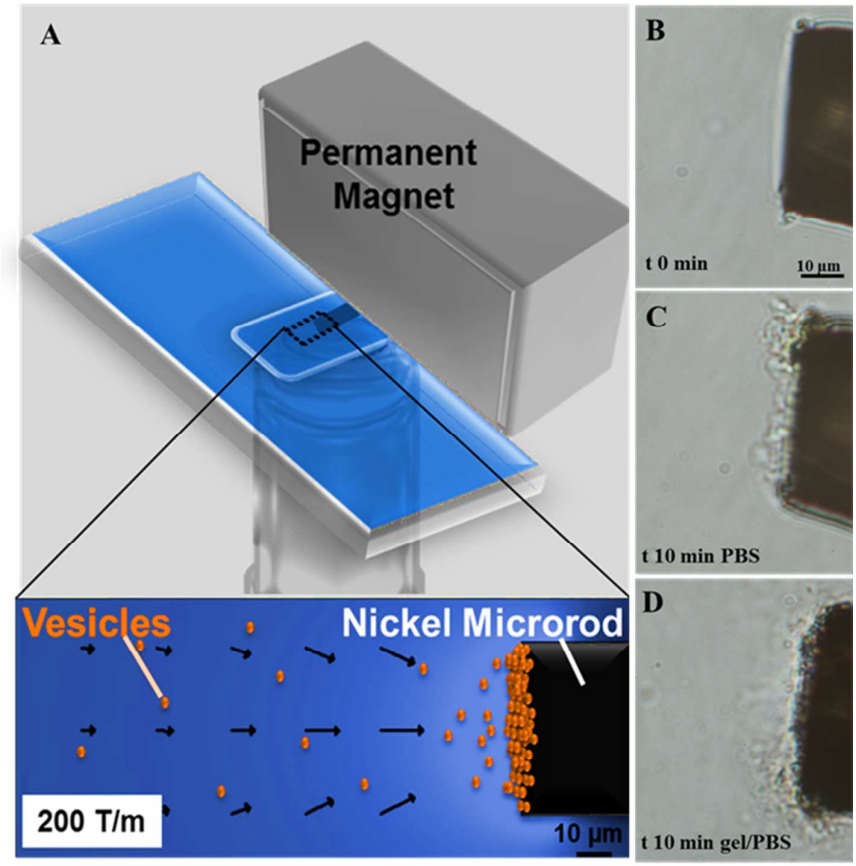

Supplementary Figure 2: Micromagnetophoresis set-up featuring a glass slide/coverslip chamber to which a 50 µm diameter nickel microrod was integrated. Magnetization of the nickel microrod was provided by a rectangular magnet positioned perpendicular to the micromagnet (A). Micromagnetophoresis experiment of EVs obtained from magnetic porcine ADSC at t 0 min (B), at t 10 min for EVs dispersed in PBS (C) and at 10 min for EVs dispersed in 1:1 mixture of Pluronic F127 gel 25% and PBS (D).

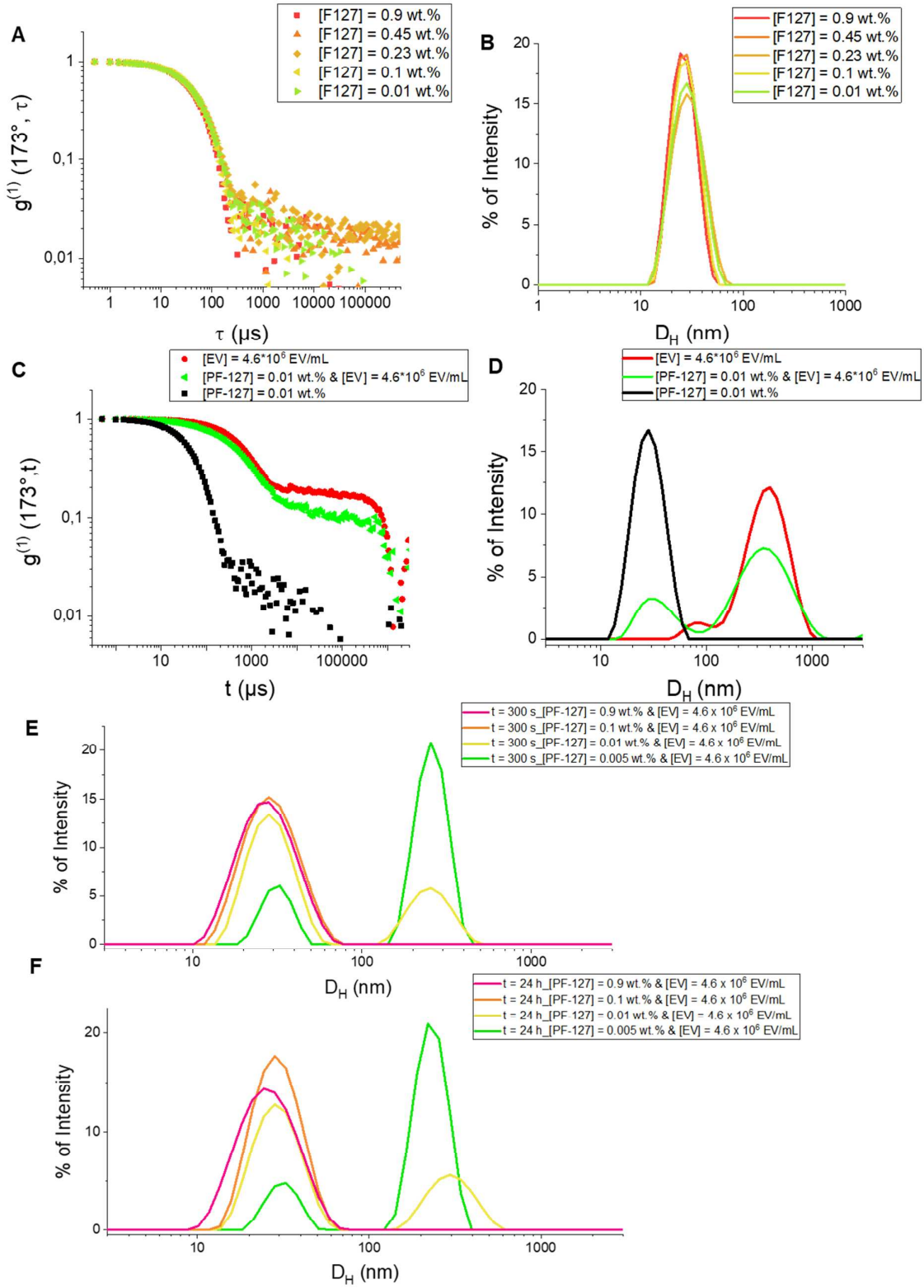

Supplementary Figure 3: Dynamic light scattering analysis of EVs and PF-127. Normalized electric field autocorrelation functions ($g^{(1)}(q,t)$ (A) and size distributions obtained by Contin analysis at 37 °C for PF-127 in PBS at different concentrations indicated in the insets (B).

Normalized electric field autocorrelation functions ($g^{(1)}(q,t)$ (C) and size distributions obtained by Contin analysis at 37 °C for PBS containing 4.6 x 10^6 EVs/mL or PF-127 at 0.01% or both (D). Size distributions obtained by Contin analysis at 37 °C for PBS containing 4.6 x 10^6 EVs/mL and PF-127 at different concentrations indicated in the insets. Measurements were performed 300 s (E) or 24 h (F) after adding EVs into PF-127 in PBS.

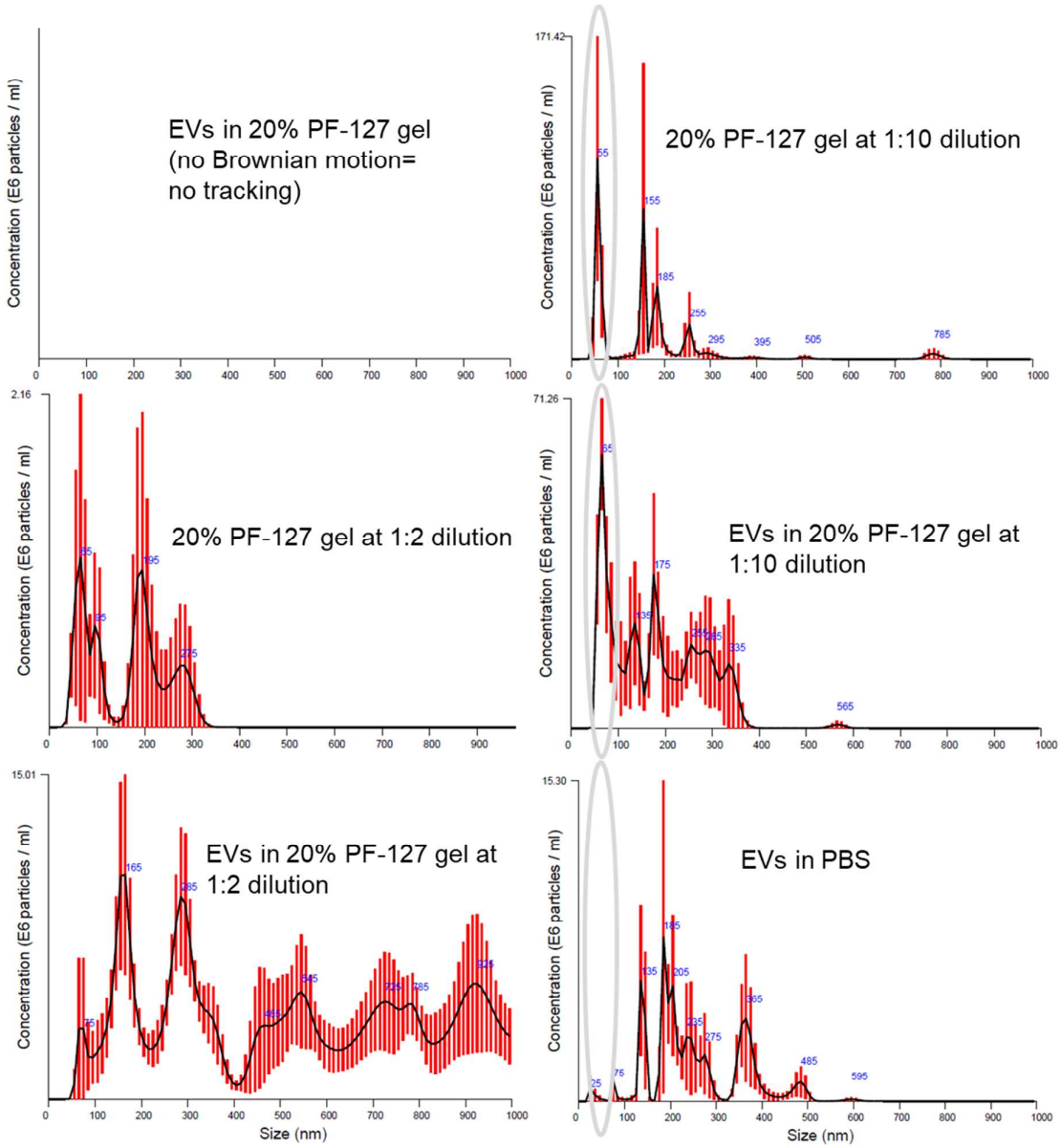

Supplementary Figure 4: Size distribution by nanoparticle tracking analysis of EVs and PF-127 gel alone or in combination at 3 gel concentration values.

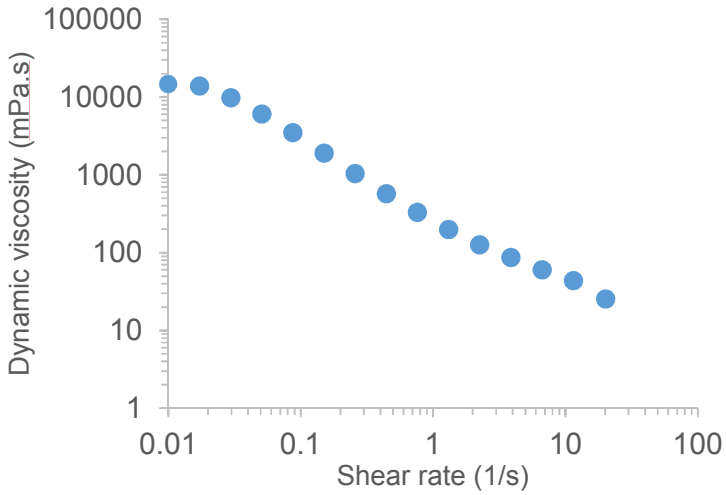

Supplementary Figure 5: Dynamic viscosity measurement at 37°C for 20% PF-127 gel at a 1:2 dilution in PBS (10% final concentration).

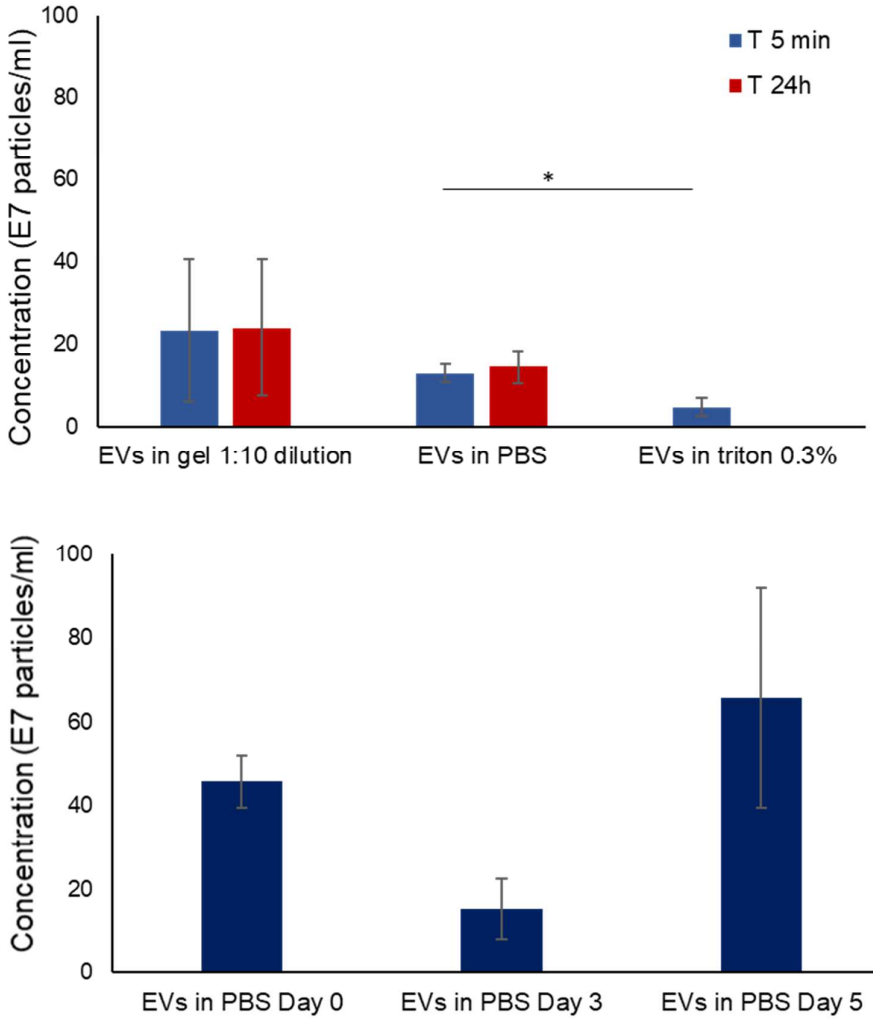

Supplementary Figure 6: Concentration determination by nanoparticle tracking analysis at 37°C for EVs in 20% PF-127 gel at a 1:10 dilution in PBS, EVs in PBS and EVs in triton X-100 at 0.3%. Measurements were performed either immediately (5 min) after suspension preparation or following a 24-hour incubation at 37°C (Upper panel). Concentration determination by nanoparticle tracking analysis at 37°C for EVs in PBS. Measurements were performed either immediately after suspension preparation (day 0) or after 3 or 5 days of incubation at 37°C (bottom panel). Bar graph represents mean ± SEM from three independent preparations. * indicate $p< 0.05$.

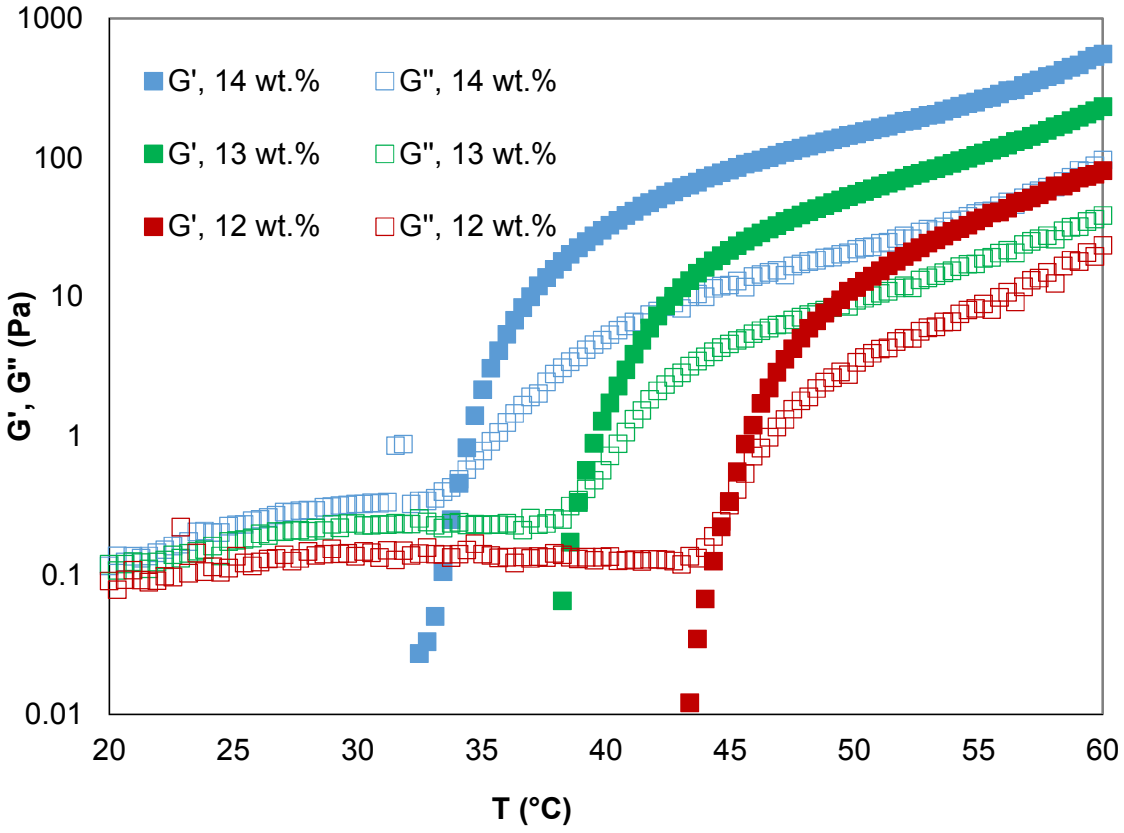

Supplementary Figure 7: Evolution of dynamic storage modulus (G') and loss modulus (G'') at a heating rate of 1°C/min from 20 °C to 60 °C for PF-127 gel at 12, 13 and 14%.

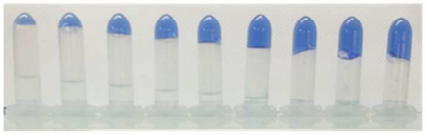
1 2 3 4 5 6 7 8 9

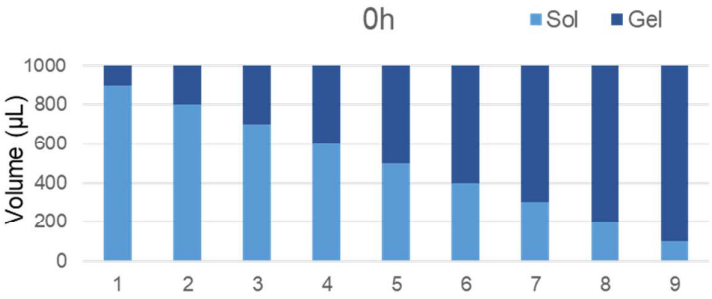
0h
Sol
Gel
Volume (µL)
1000
800
600
400
200
0
1 2 3 4 5 6 7 8 9

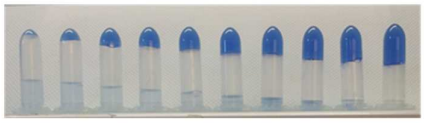

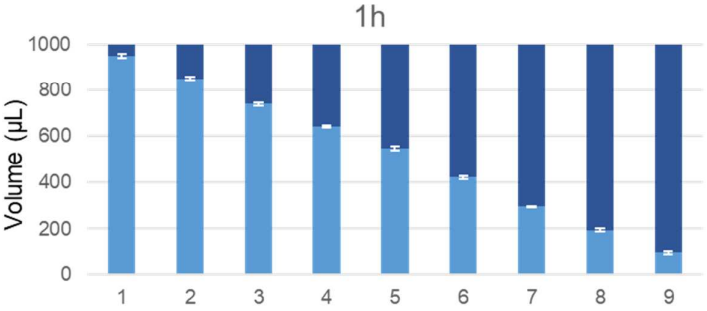
1h
Volume (µL)
1000
800
600
400
200
0
1 2 3 4 5 6 7 8 9

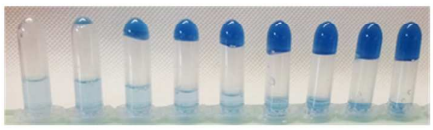

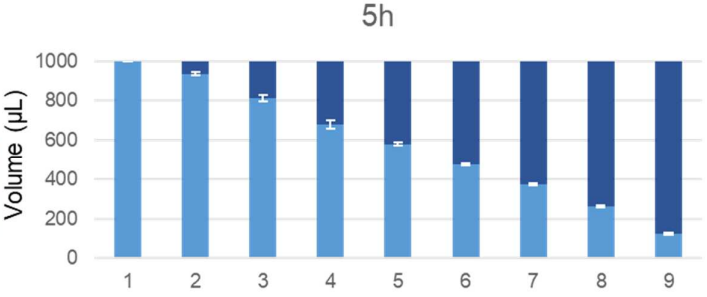
5h
Volume (µL)
1000
800
600
400
200
0
1 2 3 4 5 6 7 8 9

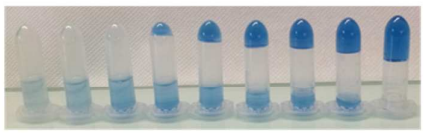

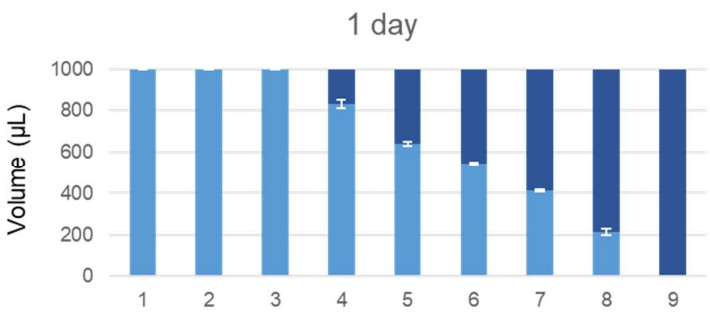
1 day
Volume (µL)
1000
800
600
400
200
0
1 2 3 4 5 6 7 8 9

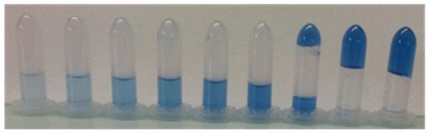

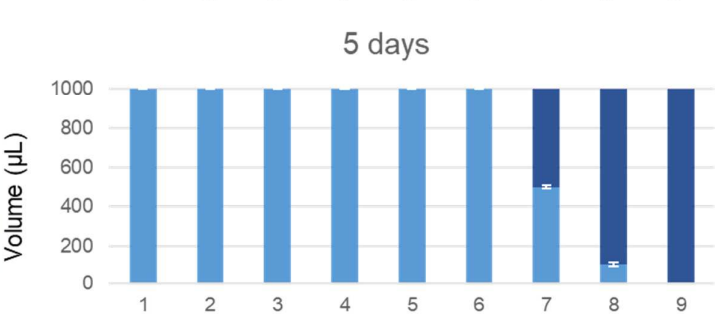
5 days
Volume (µL)
1000
800
600
400
200
0
1 2 3 4 5 6 7 8 9

Supplementary Figure 8: Evaluation of PF-127 gel dissolution kinetics at 37°C as a function of the dilution factor by tube inversion tests. PF-127 gel at 20% was diluted in PBS at serial ratios: 100 to 1000 (sample 1: 2% PF-127); 200 to1000 (sample 2: 4% PF-127); 300 to 1000 (sample 3: 6% PF-127); 400 to 1000 (sample 4: 8% PF-127); 500 to 1000 (sample 5: 10% PF-127); 600 to 1000 (sample 6: 12% PF-127); 700 to 1000 (sample 7: 14% PF-127); 800 to 1000 (sample 8: 16% PF-127) and 900 µL to 1000µL (sample 9: 18% PF-127). Dissolution kinetics was evaluated by the evolution of the sol volume as a function of the time.

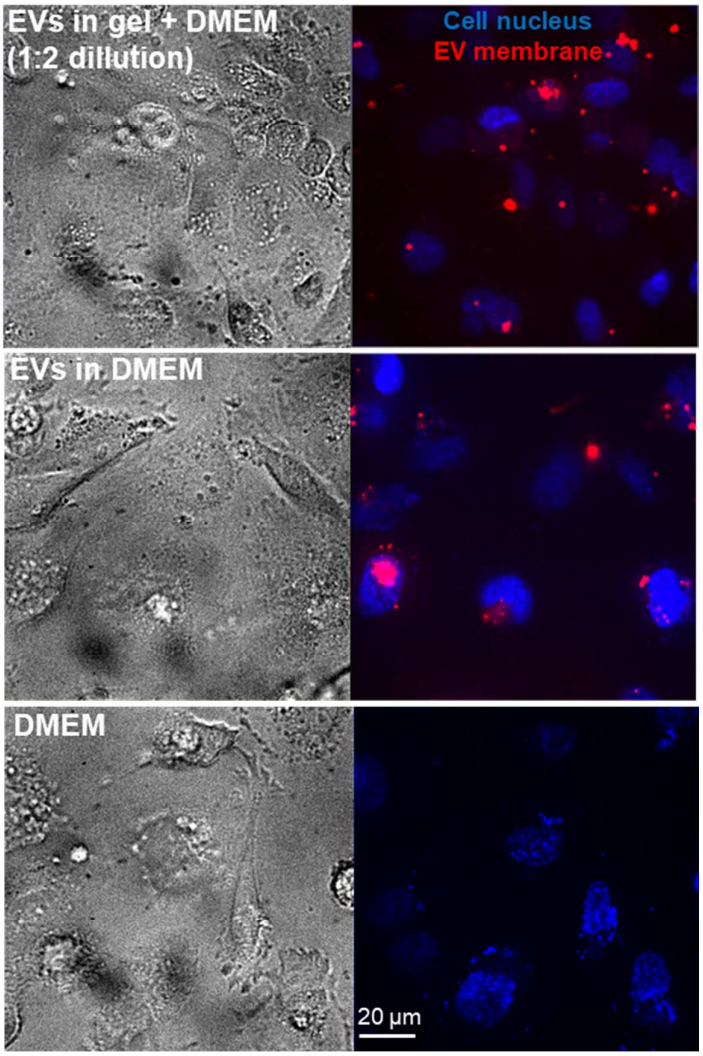

Supplementary Figure 9: Confocal evaluation of EV uptake by recipient HUVECs. EV membrane was previously stained with PKH26 dye. Images were acquired following incubation overnight with EVs in the 20% PF-127 gel in addition of complete culture medium (1:2 dilution), EVs in complete culture medium or complete culture medium alone. Recipient cells were labelled with a Hoechst nuclear staining.

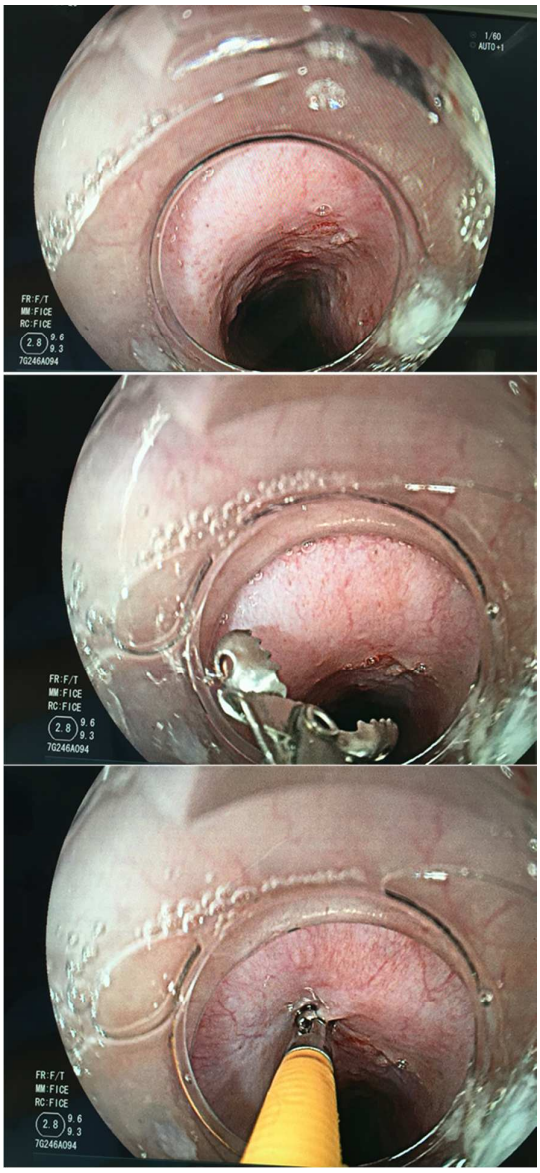

Supplementary Figure 10: Endoscopic view of swine esophagus during a biopsy to collect epithelial tissue. Biopsies were collected under animal anesthesia using radial jaw biopsy forceps.

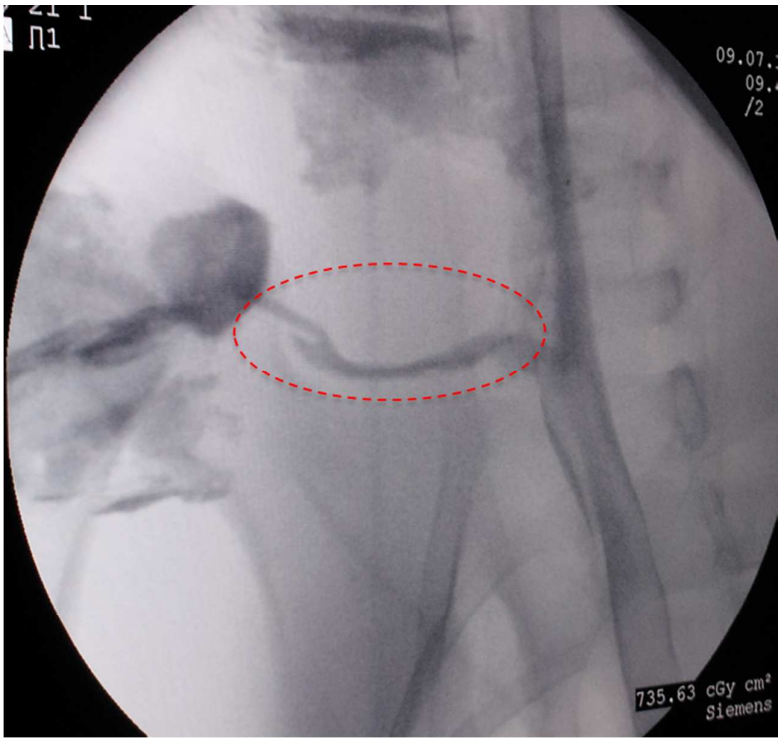

Supplementary Figure 11: Fistulography at D30 following stent ablation showing a single esophageal fistula tract (red dotted) evidenced by radiological contrast injection through the external fistula orifice.

Supplementary Figure 12: Observation of Pluronic F127 transition to a gel state (red arrows) at body temperature at the external fistula orifice and surrounding region following its administration at 4° C in liquid state.

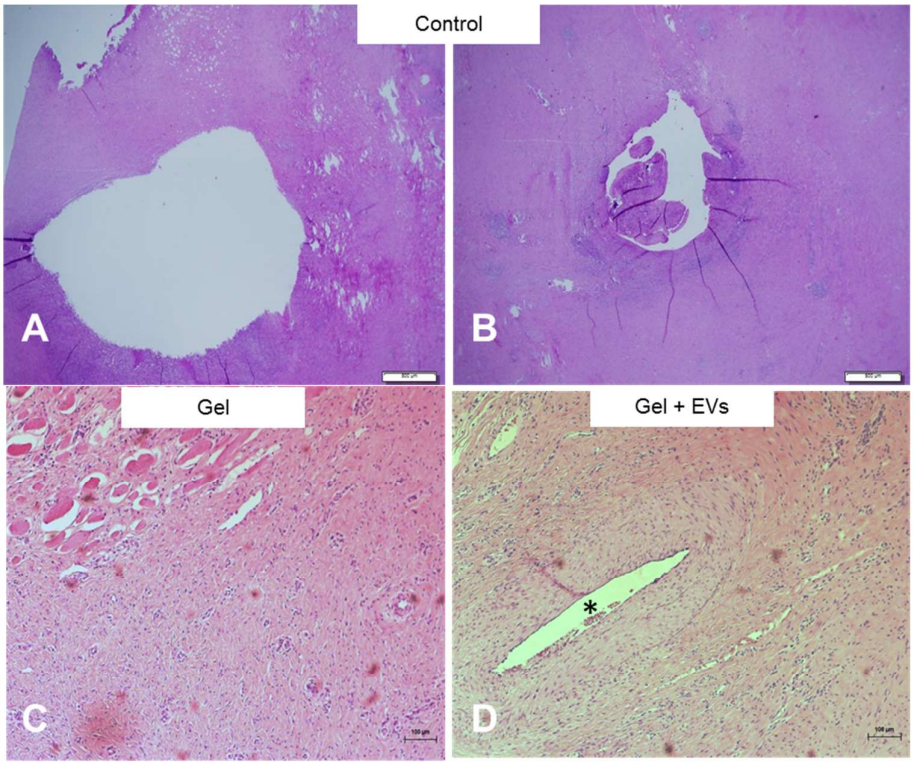

Supplementary Figure 13: Histological analysis at D45. In control group (A and B), fistulas were open with important inflammatory infiltration and fibrosis (HE, x10 for A and HE, x2 for B). Images of a closed non-inflammatory fistula tract for the gel (C) and the gel + EVs group (D). A vessel lumen was indicated by * at picture D.

Supplementary Tables

Supplementary Table 1: Cumulative 10%, 50% and 90% diameter of ADSC EVs obtained by NTA.

D10	100.3	4.53
D50	159.1	4.7
D90	269.2	11.8

Supplementary Table 2: Analysis of statistical parameters when comparing external fistula orifice closure by clinical evaluation for the control versus the gel group as well as the control versus the gel + EVs group.

Chi-square	4.381	11.00
P value	0.0363	0.0009
Odds ratio	23.40	143.0
95% confidence interval	0.8925 to 613.5	2.413 to 8476

Supplementary Table 3: Analysis of statistical parameters when comparing the absence of inflammatory aspect by clinical evaluation for the control versus the gel group as well as the control versus the gel + EVs group.

Chi-square	4.381	11.00
P value	0.0363	0.0009
Odds ratio	23.40	143.0
95% confidence interval	0.8925 to 613.5	2.413 to 8476

Supplementary Table 4: Analysis of statistical parameters when comparing internal fistula orifice closure by endoscopic evaluation for the control versus the gel group as well as the control versus the gel + EVs group.

Chi-square	12.00	11.00
P value	0.0005	0.0009
Odds ratio	169.0	143.0
95% confidence interval	2.889 to 9885	2.413 to 8476

Supplementary Table 5: Analysis of statistical parameters when comparing the occurence of complete fistula closure by radiological evaluation for the control versus the gel group as well as the control versus the gel + EVs group.

Chi-square	4.381	11.00
P value	0.0363	0.0009
Odds ratio	23.40	143.0
95% confidence interval	0.8925 to 613.5	2.413 to 8476

Supplementary Table 6: Analysis of statistical parameters when comparing the presence of a fistula tract by histological evaluation for the control versus the gel group as well as the control versus the gel + EVs group.

Chi-square	4	11.00
P value	0.0455	0.0009
Odds ratio	13	143.0
95% confidence interval	0.5110 to 330.7	2.413 to 8476

Supplementary movie 1: Time series images (750 images in 30 s) obtained by nanoparticle tracking analysis at 37°C for EVs in 20% PF-127 gel, in 20% PF-127 gel diluted 1:2 in PBS, in 20% PF-127 gel diluted 1:10 in PBS or in PBS.

Supplementary movie 2: Time series images (100 images in 10 s) obtained by confocal microscopy at 37°C for PKH26 labelled EVs in 20% PF-127 gel, in 20% PF-127 gel diluted 1:2 in PBS, in 20% PF-127 gel diluted 1:10 in PBS or in PBS.